AIAA JOURNAL
Vol. 41, No. 11, November 2003

# Simultaneous Laser-Induced Fluorescence and Mie Scattering for Droplet Cluster Measurements

Laurent Zimmer*
*National Aerospace Laboratory, Tokyo 182-8522, Japan*
Roland Domann† and Yannis Hardalupas‡
*Imperial College of Science, Technology and Medicine, London, England SW7 2BX, United Kingdom*
and
Yuji Ikeda§
*Kobe University, Kobe 657-8501, Japan*

**A technique for planar measurement of size, velocity, liquid volume, and surface area of droplet clusters in sprays and the identification of fluid flow structures, which might be responsible for droplet clustering, is reported. The technique was applied in water spray, which was injected in the airflow of burner for 0.1-MW domestic boiler. Rhodamine B dye was added in the liquid at appropriately adjusted concentration to ensure volume dependency of the fluorescence intensity. Combined droplet laser-induced fluorescence and Mie scattering images were recorded, using two charge-coupled device cameras and appropriate optical filtering. The ratio of the two light intensity images allowed measurement of instantaneous spatial distribution of droplet Sauter mean diameter. The droplet velocity field was measured by cross-correlation techniques from the Mie scattering and fluorescence intensity images and agreed well with the velocity of mean droplet diameters corresponding to the area mean diameter $D_{20}$ and volume mean diameter $D_{30}$, respectively, as measured with the phase Doppler technique. It was found that droplet clusters formed in the central region of the spray where the droplet density was high and droplet sizes small. The identified droplet clusters were tracked between time-delayed images and their displacement and cluster velocity quantified, which was in good agreement with corresponding phase Doppler measurements. In the vicinity of droplet clusters, airflow structures were identified, using particle image velocimetry, which might be responsible for the formation of droplet clusters.**

## Nomenclature

| | | |
|---|---|---|
| $d$ | = | droplet diameter, m |
| $K$ | = | constant |
| $P$ | = | pressure, Pa |
| $Re$ | = | Reynolds number |
| $V$ | = | instantaneous velocity, $m \cdot s^{-1}$ |
| $\langle V \rangle$ | = | mean velocity, $m \cdot s^{-1}$ |
| $x, y, z$ | = | Cartesian body axes, m |
| $\rho$ | = | density, $kg \cdot m^{-3}$ |

*Subscripts*

| | | |
|---|---|---|
| LIF | = | laser-induced fluorescence signal |
| Mie | = | Mie scattering signal |
| 20 | = | surface mean |
| 30 | = | volume mean |

*Superscript*

| | | |
|---|---|---|
| ‘ | = | fluctuating |

Presented as Paper 2002-0340 at the AIAA 40th Aerospace Sciences Meeting, Reno, NV, 14–17 January 2002; received 23 October 2002; revision received 19 May 2003; accepted for publication 19 May 2003. Copyright © 2003 by the American Institute of Aeronautics and Astronautics, Inc. All rights reserved. Copies of this paper may be made for personal or internal use, on condition that the copier pay the $10.00 per-copy fee to the Copyright Clearance Center, Inc., 222 Rosewood Drive, Danvers, MA 01923; include the code 0001-1452/03 $10.00 in correspondence with the CCC.

*Researcher, 7-44-1 Jindaiji-Higashi, Chofu. Member AIAA.
†Ph.D. Student, Mechanical Engineering Department.
‡Lecturer, Mechanical Engineering Department. Senior Member AIAA.
§Associate Professor, Department of Mechanical Engineering, Rokkodai Nada. Senior Member AIAA.

## Introduction

LIQUID fuels are commonly burned after being atomized to form sprays of fine droplets. Two-phase flow combustion involves different interacting processes such as chemistry-heat exchange, turbulent multiphase flow dynamics, evaporation, and mixing. One of the difficulties arises from the existence of different diameters of droplets, leading to different dynamic behavior of droplet dispersion, evaporation, and turbulent interaction with the surrounding gas. This leads to an important problem: the instantaneous spatial distribution of droplets in sprays might have dense and dilute regions, characterized by the appearance of clusters of droplets,[1,2] which can lead to the formation of fuel-rich and lean regions. Such droplet clusters can appear in nonevaporating sprays, governed only by gas fluid motions[3] or the atomization process.[4] During combustion, the process is more complicated, and the presence of droplet clusters might be either caused by droplet interaction with flow turbulence and/or preferential evaporation and flame propagation. Stricter emission regulations from combusting systems requires better understanding and control of the instantaneous structure of liquid fuel sprays rather than the time-averaged structure, which has been commonly used till now.

The study of the formation of such droplet clusters requires simultaneous measurement of diameter and velocity in a plane. From the experimental point of view, the most widely used system is the phase Doppler anemometer,[5] which is an extension of laser Doppler velocimetry with monitoring of sizes by using three photomultipliers. This technique has two main drawbacks: it provides measurements at a point, and it is not applicable in dense sprays, where more than one droplet can exist in the probe volume. It is possible to overcome these drawbacks by using imaging techniques. However, planar measurements of droplet diameter and velocity must be available, and different approaches have been proposed. One droplet-sizing approach is to measure the total amount of light scattered by a droplet, which is illuminated by a continuous laser [streaked particle image velocimetry (PIV[6])] and with a proper calibration to relate it to the diameter of the droplet. This technique

suffers from the nonuniform intensity of the incident laser sheet and is affected by attenuation of the laser light intensity caused by the interaction of the laser sheet with optical windows or the droplets in dense sprays. Another technique consists in using a double-pulse laser to measure the size of the images of droplets[7] together with a particle tracking approach for velocity measurement, but this is valid for droplets larger than 100 $\mu$m and for dilute sprays, where individual droplets can be distinguished. To measure the size of small droplets with a better accuracy with this approach, a back-lighting technique has been suggested.[8] To overcome problems of out-of-focus droplets, the boundaries of the droplets are determined using edge detection. A threshold on the sharpness of the boundary is used to determine the amount of deviation from the focal plane and therefore to relate the size measured to the real size of the droplet. Nevertheless, this technique remains applicable only in dilute sprays, where no overlapping of droplets is to be expected, while problems with the edge detection of droplet boundaries remain and introduce uncertainties. The use of the interferometric pattern formed by the light scattered from droplets, following illumination by a laser sheet and out-of-focus imaging, is a good alternative. The size is measured from the fringe spacing of the interferometric pattern.[9] This technique can measure in relatively dense sprays, provided that physical image compression (with lenses) is used, so that the observed interferometric pattern is limited to few lines on the charge-coupleddevice (CCD) camera detector.[10] This technique has the advantage of being insensitive to the incident laser light intensity, but is limited to spherical droplets. Another droplet sizing technique, which is less sensitive to variations of the incident light intensity and can measure directly Sauter mean diameter in dense sprays, is available. This technique relies in measuring with laser-induced fluorescence intensity emitted from dyed droplets the liquid volume of droplets and with the scattered light (Mie) intensity the liquid surface area. This technique is known as planar droplet sizing or laser sheet dropsizing[11,12] and makes use of the ratio between the fluorescent and scattered light intensities to obtain the Sauter mean diameter (SMD) according to Eq. (1):

$$\mathrm{SMD}(x, y) = k \frac{I_{\mathrm{LIF}}(x, y)}{I_{\mathrm{Mie}}(x, y)} \tag{1}$$

Because the ratio of intensities is used, the sizing information is insensitive to incident laser intensity variations. The limitation and uncertainty in determining the droplet SMD have been evaluated, and appropriate data-processing methods have been suggested.[13,14]

For the measurement of droplet velocity in sprays, different algorithms have been developed, usually based on particle imaging velocimetry associated to a double-pulsed Nd:YAG laser. They all tend to take into account the relation existing between the velocity and the diameter of the droplet. If the spray is dilute, particle tracking velocimetry[7] is the best choice, as it will measure individual velocity. For dense sprays this tracking is impossible, and one should look for statistical quantities. One algorithm is the so-called multilayer intensity. The original digital images are divided into three subimages,[15] representing respectively the low, medium, and high level of scattered light intensity from the droplets. This division is intended to give the velocity of small, medium, and large droplets, assuming constant laser sheet intensity through the region seen by the camera. No measurement of the droplet sizes is possible, and furthermore, no differentiation can be done between a single large droplet and a group of small droplets, which is desirable in two-phase flow measurements. However, PIV can provide some useful information on spray dynamics. It has furthermore the advantage of providing instantaneous two-dimensional information that can be used to characterize spray unsteadiness.

This paper intends to apply a planar-droplet-sizing technique coupled to PIV to study the instantaneous and time-averaged characteristics of a spray in a practical burner. It demonstrates the quantities that can be measured together with a discussion concerning uncertainties and limitations. For the measurement of the diameter, the planar-droplet-sizing technique is applied with simultaneous monitoring of fluorescence and elastic scattering to get instantaneous Sauter mean diameter information, as presented in Ref. 16. Two cross-correlationCCD cameras allow velocity measurements, using PIV algorithms, from the fluorescing and scattered light intensity images. The ability of the technique to characterize droplet clusters on instantaneous spray images and identify the associated air flow structures is presented.

The rest of the paper is presented in five sections. The next section describes the experimental arrangement and instrumentation. The third section presents the spray characteristics in terms of droplet size and velocity as measured by phase Doppler anemometer, which are used as a reference for the planar-droplet-sizing technique. The fourth section shows the planar spray measurements and presents the measured SMD and velocity and compares it with the phase Doppler measurements. Also, it examines the formation of instantaneous droplet clusters and the instantaneous airflow velocity field that might be responsible for their formation. Finally, the instantaneous velocity and SMD of droplet clusters is quantified and compared with size-velocity correlations measured by phase Doppler anemometer. The paper ends with a summary of the main conclusions.

## Experimental Apparatus

### Spray

A practical gun-type burner was used for the present study, and a detailed sketch of the nozzle is depicted in Fig. 1. The spray characteristics of this type of injector have been studied.[17] The water pressure is set to 0.7 MPa giving a flow rate of 9.46 l/h, which corresponds to the heat release of 0.1 MW, when operating under reacting conditions with kerosene fuel. The airflow rate is set to 110 $\mathrm{Nm^3 \cdot h^{-1}}$, which gives a velocity $V_{\mathrm{air}} = 14.7\ \mathrm{m \cdot s^{-1}}$ and a Reynolds number based on the effective diameter of airflow $Re_{\mathrm{air}} = 1.67 \times 10^5$. The ratio between the momentum flux ($\rho$mV) from the water and the air is 0.124. The combination of the nozzle and the baffle plate generates a recirculation zone in the airflow,[18] which is used to stabilize the flame. Because the ratio between the mixing and chemical timescales is lower than 1 (estimated to be of the order of $10^{-3}$ in the case of domestic fuel according to[18]), the flame holder is necessary.

In the present application water was injected, and therefore all of the tests are performed in isothermal, nonevaporating conditions. Rhodamine B is added to water with a concentration of 0.0089 g/l to get the fluorescent intensity and ensure that the fluorescence intensity is proportional to liquid volume.[13] There are two reasons for this choice. The first is that studies in isothermal conditions avoid problems associated with fuel evaporation, which can modify the calibration of the technique. The second is that Rhodamine B is not directly miscible in fuel and requires extra chemical species for mixing. Because the purpose of our study was to evaluate the planar-droplet-sizing technique and understand the origin of droplet clusters in sprays, using water did not influence our conclusions.

### Image Recording

Two CCD cameras (TSI PIVCAM 10-30, cross-correlation, $1000 \times 1016$ pixels, Kodak ES1.0) are used with a lens of 60-mm focal length to record simultaneously images of Mie scattering and laser-induced fluorescence (LIF) intensities. A dual-cavity Nd:YAG

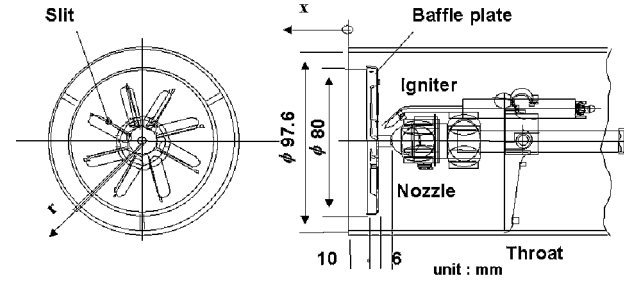


**Fig. 1 Sketch of the nozzle.**

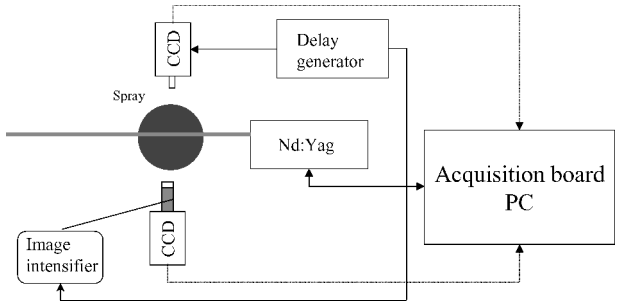


**Fig. 2 Sketch of the global facility.**

laser (SP PIV-400, 400 mJ per pulse with a wavelength of 532 nm) forming a laser sheet of less than 1 mm thickness is used as laser source with a typical pulse duration of 8 ns. The cameras were placed perpendicular to the laser sheet to avoid optical distortion. One of the cameras is equipped with an optical filter (XF3019605DF50 from Omega Optical that has a total bandwidth of 50 nm centered on 615 nm), removing the scattered light and allowing only the fluorescent signal to pass. Because the fluorescence intensity is much weaker than scattered light, a high-speed gated Image Intensifier Unit C6653 from Hamamatsu is used. During the experiments, its amplification is set to 95% of its maximum, and the gate time (set to 50 $\mu$s, the minimum value available for the cameras) is synchronized with the laser pulses to avoid a strong background noise and to obtain the corresponding two instantaneous images (Fig. 2). The remaining background noise is caused by the intensifier of the CCD camera because the measurements were obtained in a dark room. The addition of the intensifier modifies the optical properties of the receiving cameras, and therefore specific calibration has to be done to ensure identical field of view and magnification for both cameras. This is done using a reference particle image and performing cross-correlation between the images recorded with the two cameras. Mechanical displacement of the cameras is performed until the maximum displacement measured by cross correlation is below 30 pixels (which represents 3 mm). The remaining misalignment is corrected during image processing for translation/rotation effects, as quantified by the cross correlation of the images of a calibration target. The final misalignment between the two simultaneous images is down to less than a pixel, which corresponds to a physical space of around 50 $\mu$m.

## PDA Measurements of Spray Characteristics

PDA measurements were performed to obtain time-averaged velocity and SMD maps of the water spray. A Dantec Phase Doppler Velocimeter was used. A dual-beam system comprised a 5W-$Ar^+$ laser and a conventional fiber-optic PDA with a 40-MHz Bragg cell for frequency shift and a 500 mm focal length front lens. The receiving angle was 30 deg forward scattering, which led to a high data rate. The mean arithmetic velocities as well as the SMD are plotted in Fig. 3. Two important observations are identified from those measurements. The first one is that the range of SMD is quite large, varying from 15 to 46 $\mu$m. Therefore, it is a good test for the planar-droplet-sizing technique to check if it is able to detect those differences. The second is that larger droplets are found at the edge and smaller droplets are entrained in the central region of the spray.

One can further notice the existence of an airflow-recirculating zone characterized by the presence of small droplet diameters. This region comes from momentum exchange between spray and the airflow surrounding the gun-type nozzle. The recirculation is also present when no air is supplied or when no droplets are discharged, but its magnitude and location is a function of the two momentum fluxes. The velocity presented in Fig. 3 corresponds to the arithmetic mean velocity as measured by PDA based on either 20,000 samples (in the core of the spray) or 5 min (at the edge, where the droplet concentration is small). The Stokes number is the ratio between the aerodynamics response time of the droplet ($Stp = \rho d_p^2/18\mu$ in case of Stokes drag) divided by the timescale of the airflow. The droplets with a diameter smaller than 25 $\mu$m have a Stokes number lower than 1. Their aerodynamic response time is 3.5 ms, whereas the droplets of 50 $\mu$m have a response time of 13.9 ms. The timescale of the gaseous flow is estimated to be 6 ms, which gives a Stokes number of 0.6 and 2.3, respectively, for 25- and 50-$\mu$m droplets. Therefore, 25-$\mu$m droplets are expected to follow the airflow recirculation zone, whereas the larger droplets do not.

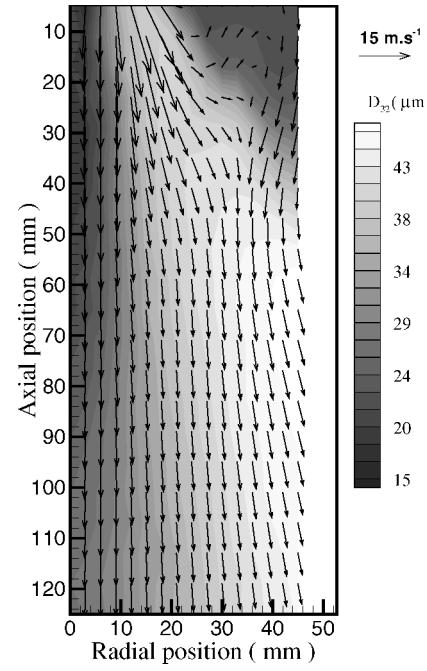


**Fig. 3 PDA results for water spray.**

## Planar Spray and Flow Measurements

### Typical Instantaneous Image

Figure 4 illustrates a typical Mie-scattering image recorded in the present experiments. In contrast to the laser-induced fluorescent images (right side), one can observe the core of the spray and especially the presence of branchlike structures, which is the major interest in the present study. On the LIF images one can see that mainly the edges of the spray are recorded, corresponding to larger droplet diameters and liquid volume (as measured by PDA) and therefore higher fluorescence intensity. The outer boundary of the liquid volume of the spray can be easily identified on those images, which can identify the spray ejection angle, which was of the order of 60 deg for the current operating conditions. Those two figures illustrate the main difference between Mie scattering and LIF images, as they identify different quantities. A hollow cone spray is formed, which has larger droplets and liquid volume away from the centerline and a large number of small droplets (therefore low SMD) and large surface area close to the centerline. The planar measurements of Fig. 4 confirm the expected spray structure.

### Measurements of SMD Distribution

The intensity ratio of the instantaneous fluorescent and Mie-scattering images is computed. This ratio is proportional to the Sauter mean diameter of the droplets.[11] The calibration constant between SMD and intensity ratio was determined with a monodisperse droplet generator (creating droplets of 120 $\mu$m). The laser illumination and the operating conditions of the image intensifier were set at the same level as those used for measurements in the spray. The determination of the constant can also be done using the PDA results. However, in general, the planar measurements should be done independently of phase Doppler measurements, and a separate calibration is required. The intensities were calculated in interrogation windows of $8 \times 8$ pixels, corresponding to $0.85 \times 0.85$ mm. A typical instantaneous measurement of SMD is shown in Fig. 5. This figure shows that the spray is characterized by a central region with small SMD, as expected for a hollow cone spray.

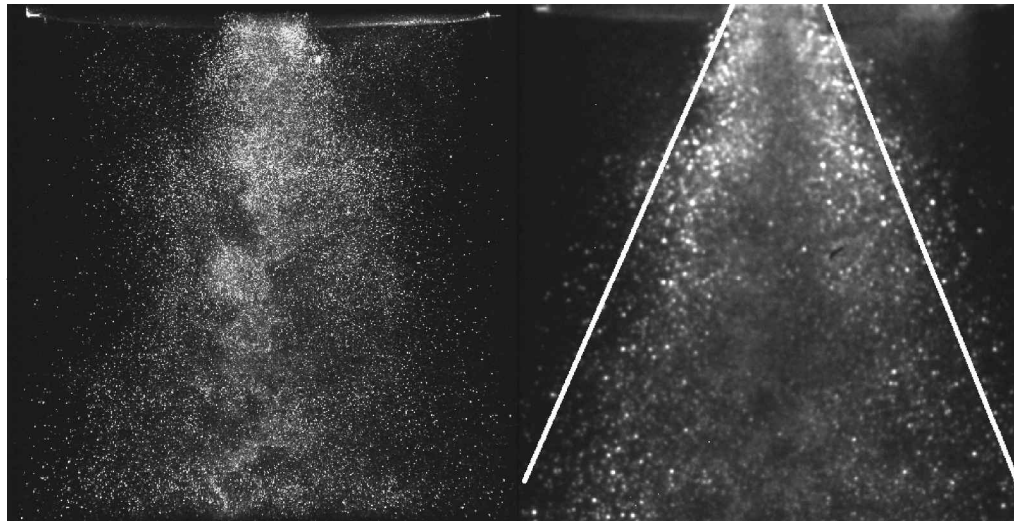

**Fig. 4 Typical instantaneous Mie-scattering and LIF images.**

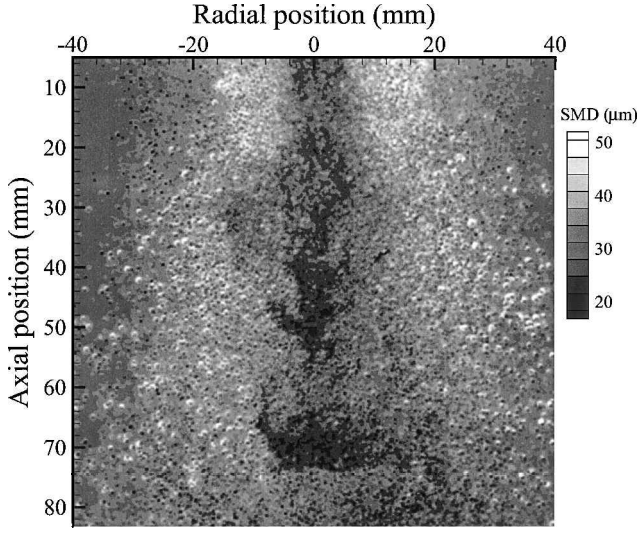


**Fig. 5 Instantaneous SMD map.**

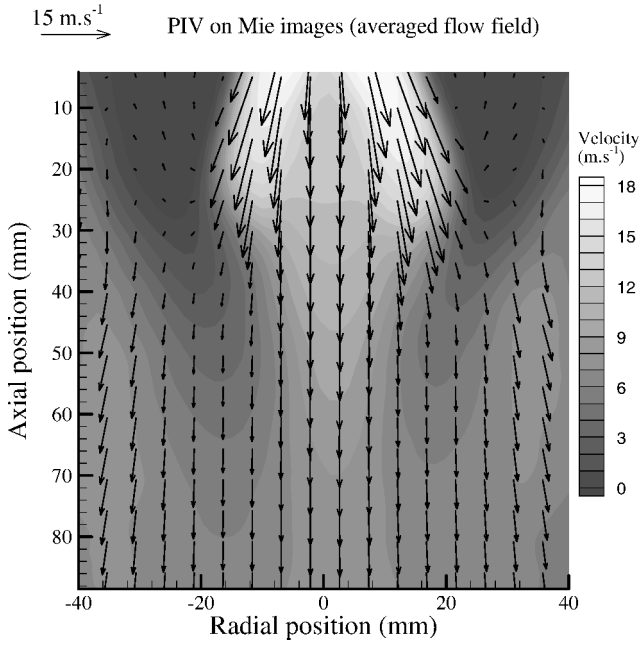


**Fig. 6 Mean velocity profile on Mie-scattering images.**

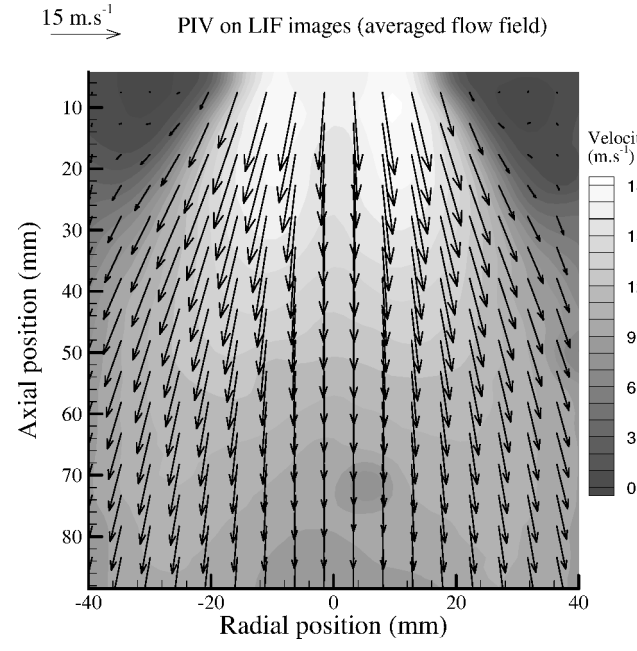


**Fig. 7 Mean velocity profile on LIF images.**

**Cross Correlation**

PIV algorithms were used to measure the droplet velocity in the spray. The time delay between the two pulses is set to 50 $\mu$s providing a typical displacement of the order of 8 pixels between the two images. To retrieve the velocity, the TSI software Insight 3.1 is used. The so-called Hart correlation[19] is chosen with initial window of $64 \times 64$ and final window of $16 \times 16$ pixels. This window size corresponds to a physical spacing of 1.6 mm. Using windows of $8 \times 8$ pixels might not necessarily improve the results as, in this case, the correlation peak might be biased by the presence of a peak of intensity representing the displacement of this specific droplet or group of droplets. The aim here is to have an insight of the typical time-averaged velocities and compare them with PDA measurements. However, it is not possible to know exactly the number of droplets participating in the correlation, as the spray is quite dense, and no individual droplets can be observed in the dense part of the spray. A first validation is performed on the expected ranges of velocity to avoid obviously wrong vectors. The average velocity field is computed on the basis of 800 instantaneous images on both Mie-scattering images (Fig. 6) and LIF images (Fig. 7).

The mean velocity fields obtained from LIF images $\langle V_{\mathrm{LIF}} \rangle$ and Mie images $\langle V_{\mathrm{Mie}} \rangle$ exhibit different behavior. To illustrate the main

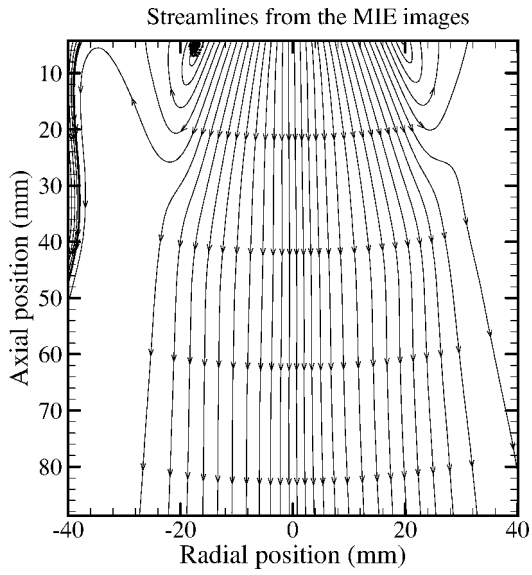


**Fig. 8 Trajectories from Mie vector field.**

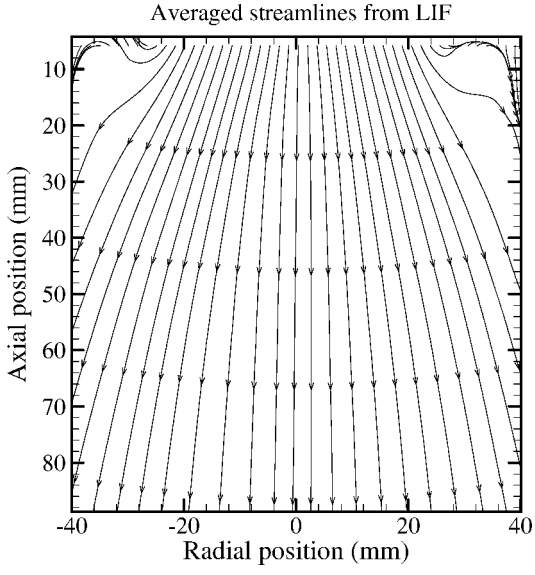


**Fig. 9 Trajectories from LIF vector field.**

differences, the trajectories of the droplets as measured by the mean velocity are shown in Figs. 8 and 9. One can mainly see two differences. The first is that the trajectories calculated by the Mie-scattering images exhibit a strong recirculation region close to the exit. This depicts the movement of small droplets interacting with the airflow. This recirculation can hardly be seen on the trajectories calculated by the LIF images, as those trajectories represent large droplets, which have a higher response time, and do not follow the airflow. The second important conclusion is that no clear radial expansion can be seen on the Mie-scattering streamlines, whereas it can be detected on LIF streamlines. The interaction between the airflow and the droplets is the explanation for this difference, as large droplets will tend to be less influenced by the air momentum and, therefore, cannot follow the airflow recirculation zone.

To understand the physical data recorded, it is important to compare with data based on PDA measurements. As presented in Fig. 10, one can see that the velocity measured from the LIF images $\langle V_{\mathrm{LIF}} \rangle$ is close to the mean droplet velocity, which has been computed with a volume $d^3$ weighting of the PDA velocity measurements, which should be associated with the velocity of the volume mean diameter $d_{30}$. This illustrates the fact that LIF imaging is proportional to the volume of the droplets. On the other hand, the velocity measured

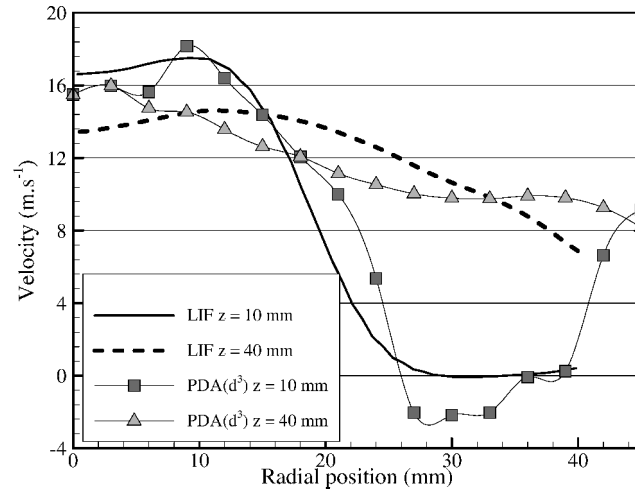


**Fig. 10 Comparison between PDA and LIF velocity.**

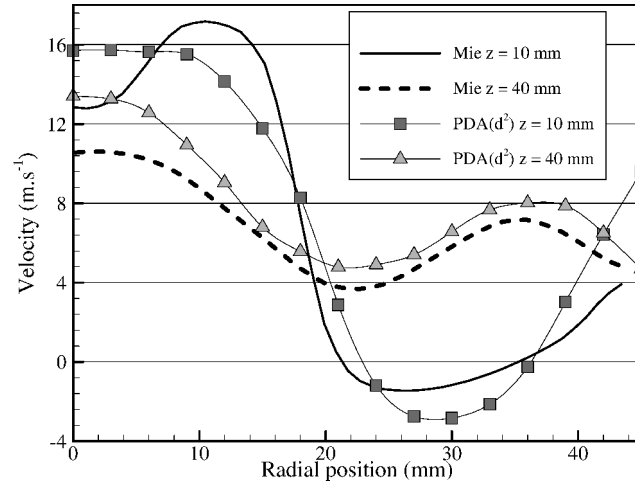


**Fig. 11 Comparison between PDA and Mie velocity.**

from the Mie images $\langle V_{\mathrm{Mie}} \rangle$ shows good correspondence with the droplet velocity from the PDA measurements computed with droplet surface area $d^2$ weighting (Fig. 11), which should be associated with the velocity of the area mean diameter $d_{20}$. The larger discrepancy between velocities at the edge of the spray, measured from PLIF images rather than Mie images relative to PDA measurements, is caused by the dynamic range of the cameras. The cameras have an intensity dynamic range of 8 bit, allowing the detection of fluorescence intensity from single droplets with diameter between 60 and 15 $\mu$m before saturation occurs. The corresponding diameter range for the scattered light intensity is between 60 and 8 $\mu$m. Therefore, PLIF intensity at the edge of the spray, where the droplet density is lower than in the main part of the spray, will be biased toward larger droplet diameters, and therefore larger velocity, because the gain of the camera was adjusted to detect without saturation the main dense part of the spray. This also explains why the recirculation zone is not captured when applying PIV on PLIF images. Therefore, the velocity measured by the cross-correlation methods of the instantaneous time-delayed pairs of intensity distributions from Mie and LIF images can provide measurements of velocities in agreement with the velocities measured by the PDA after appropriate weighting with the droplet surface area and volume respectively.

### Eduction of Flow Eddies

The flow structures, which might be responsible for the presence of droplet clusters in the spray, can be investigated. Because PIV gives an instantaneous velocity field, it is possible to detect structures within the flowfield. To detect vortex like flow structures, the method of the complex eigenvalues of the two-dimensional tensor of the

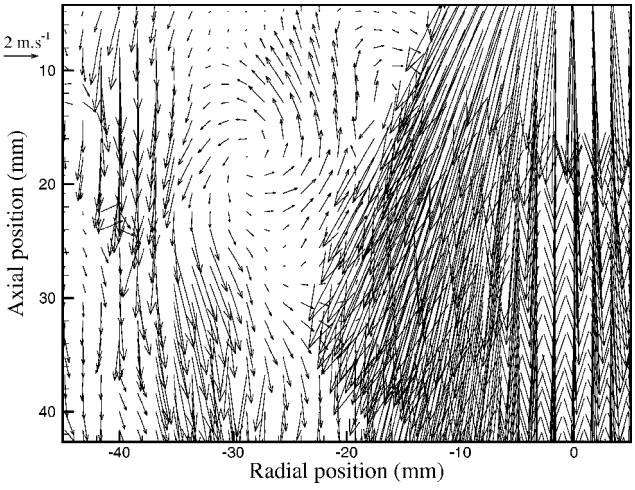


**Fig. 12 Example of an eddy within the burner exit.**

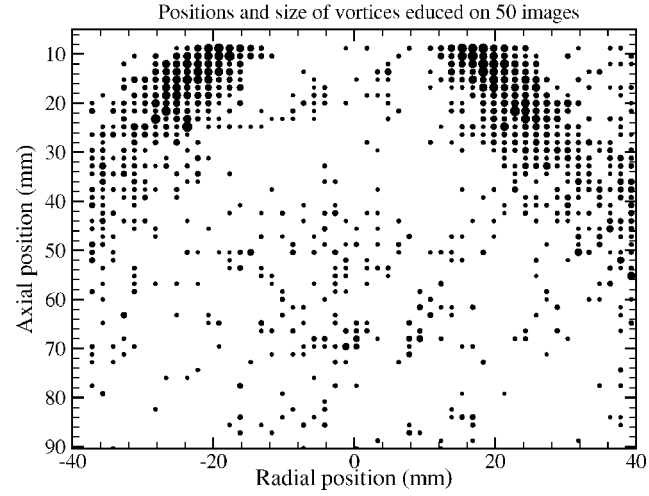


**Fig. 13 Positions of eddies.**

gradient of velocity is used, as introduced in Ref. 20 and further reported in Ref. 21 and recently Ref. 22.

As the PIV results correspond to a uniform grid, it is possible to compute easily the vorticity using a Richardson interpolation scheme,[23] which is third-order accurate and is

$$\omega_{i,j} = \frac{V_{i-2,j} - 8V_{i-1,j} + 8V_{i+1,j} - V_{i+2,j}}{12\Delta x} - \frac{U_{i,j-2} - 8U_{i,j-1} + 8U_{i,j+1} - U_{i,j+2}}{12\Delta y}$$

where $i$ and $j$ represent the indices along the lines and columns respectively and $\Delta x$ and $\Delta y$ represent the spacing between the PIV vectors.

These complex eigenvalues are combined with the existence of a peak of vorticity to retrieve the center of the structure. It is important to combine both peaks in order to avoid the shear stress being the source of a flow eddy. Flow eddies are deduced from the Mie-scattering instantaneous velocity fields because they represent the movement of small droplets. It is expected that the calculated flow velocity field from the Mie-scattered images might deviate from the airflow field. However, the calculated velocity from the Mie images is mainly weighted toward the small droplets, which follow fairly well the airflow field, and, therefore, is expected to provide a good representation of the airflow structure. A typical example of such a flow structure can be seen in Fig. 12. This typical flow structure is present at the edge of the spray and close to the baffle plate.

Flow structures can also be identified on LIF images, but their position is slightly different from the Mie-scattering images. This is because the larger droplets might have a Stokes number of the order of one for different local airflow conditions than the smallest droplets, and, therefore, LIF images would not be representing the airflow.

When detecting flow eddies representing the airflow field, attention has to be paid to the accuracy of the measurement, especially by checking whether the result is physical. The uncertainty in PIV algorithms is typically 0.1 pixel of the measured velocity. When applying PIV in sprays, the effect of the size distribution cannot be neglected, as correlation between size and velocity exists. For the region where a vortexlike flow eddy is found, the PDA results showed a value for $d_{20}$ of about 20 $\mu$m. Knowing that Mie scattering is close to the velocity of $d_{20}$, the Stokes number of 20 $\mu$m droplets will show whether the information retrieved is meaningful. The identified flow eddies have typically a velocity of $0.4 \pm 0.1$ m $\cdot$ s$^{-1}$. Its size represents typically six interrogation windows, hence a length of $10.0 \pm 1.7$ mm. Therefore, its characteristic time is of the order of $25 \pm 7$ ms. Water droplets of 20 $\mu$m have an aerodynamics response of 3.5 ms. Therefore, it can be concluded that the flow eddies found should represent quite well the airflow. However, the strength of those eddies is not precise because the displacement involved is of the order of 0.4 pixels, which gives at least an uncertainty of 25% on the measured velocity. The sizes of the flow structures indicated here are relative sizes because no absolute values can be deduced for the airflow from the Mie images. The size reported in Fig. 13 is based on the computed strength of the eddy, as being the complex part of the eigenvalues, which is defined as being the swirling strength.[22] The instantaneous positions of the identified flow structures can vary significantly, and Fig. 13 shows the location of the center of these structures within the flow on a basis of 50 images. The number of images is limited to 50 for clarity reasons. Figure 13 indicates the following. The most probable region for the location of the flow eddies is close to the nozzle and away from the centerline, where the injection of droplets interacts with the airflow in the wake of the baffle plate. In the central region of the spray, flow eddies also appear but at a lower probability. It is interesting to check whether the location of these flow eddies is associated with the formation of droplet clusters in the spray.

### Cluster Tracking Velocimetry

When looking at the Mie-scattering images (see Fig. 14), one can identify regions of higher intensity, which indicate high droplet surface area. These regions are defined as droplet clusters. The droplet clusters correspond to regions of high droplet density with a low SMD.[24] The present study attempts to understand the dynamics of such regions. The first task consists in determining their exact position on the two successive (in time) pair of images. As seen in Fig. 14, the clusters can be easily identified on the Mie-scattering images, using adaptive threshold to binarize the image. The possibility to use Mie scattering to identify droplet clusters has been previously reported.[1]

To avoid spurious effects of the level of binarization, the total LIF intensity of the first cluster is computed, representing the liquid volume of the droplets in the cluster. The threshold on the second image is adapted to ensure the corresponding liquid volume identified by the LIF intensity is present in the cluster, ensuring the tracking of the same volume of liquid. The liquid volume is computed by summing the intensity of the LIF images. Typical clusters have a size of more than 200 pixels corresponding to an equivalent area of a 5 mm square, so that the evaluation of the volume is quite reliable. The centroid is the center of gravity of the cluster. The shape of the cluster remains similar because the time delay between two consecutive images was 200 $\mu$s.

One important bit of information that is possible to obtain is the probability to find a droplet cluster as a function of the spatial coordinates. By taking the average over 800 images, it is possible to define the normalized probability density function (PDF) as representing the typical positions of the clusters. A grid of $10 \times 10$ is used with a space step of 1 cm. Each time a cluster is found, its coordinates are stored inside the Cartesian grid. The results presented in Fig. 15

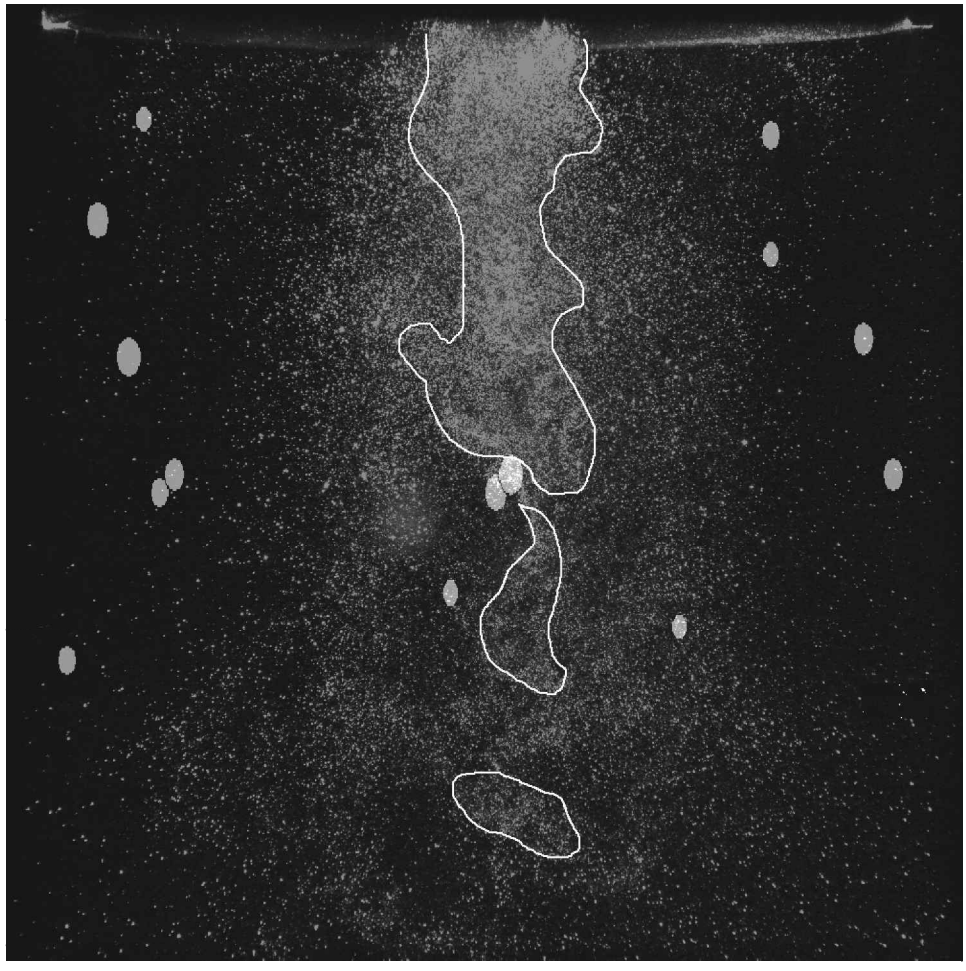

**Fig. 14 Original Mie-scattering image; position of eddies and clusters.**

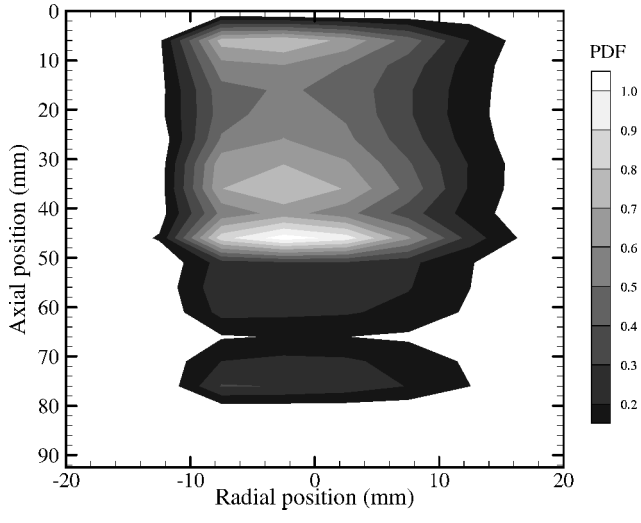


**Fig. 15 PDF for the position of the clusters.**

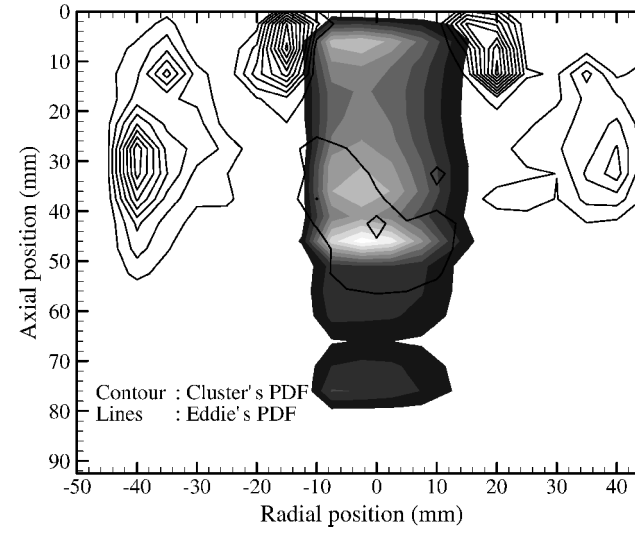


**Fig. 16 Comparison between the PDF of clusters (color) and swirling motions (lines).**

identify two distinct regions. The first one corresponds to a distance less than 5 cm from the nozzle exit and is associated with a high probability of finding clusters of droplets. The second one is located at an axial distance larger than 5 cm and exhibits a relatively low probability of finding droplet clusters. When plotting together the PDF for droplet clusters and for presence of flow eddies in Fig. 16, one can notice the presence of a link between the two distributions. The PDF of the cluster is shown in contour, whereas the isolines represent the PDF of the swirling eddies. One can observe that isolines are around the peak in the contour, suggesting a link between the two PDF.

The accuracy of the tracking algorithm highly depends on the definition of the cluster center and on the time delay between the two pulses. Experiments have been done for that purpose with a time delay of 200 $\mu$s (which is four times larger than the one used for PIV results) to have a better accuracy. The centroid of the cluster is taken as the reference for determining the displacement and therefore the

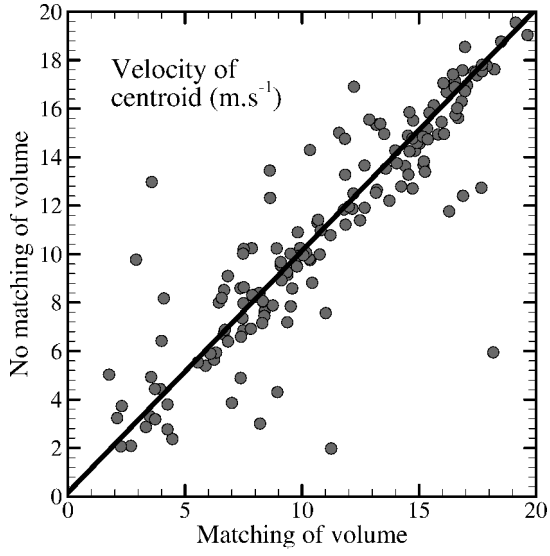


**Fig. 17 Influence of matching volume on centroid's displacement.**

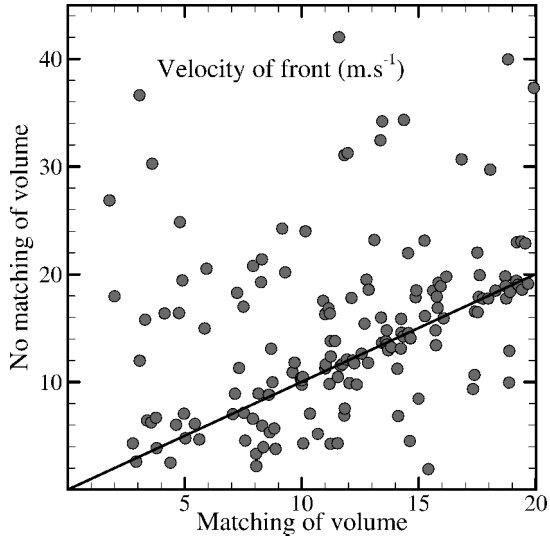


**Fig. 18 Influence of matching volume on front boundary displacement.**

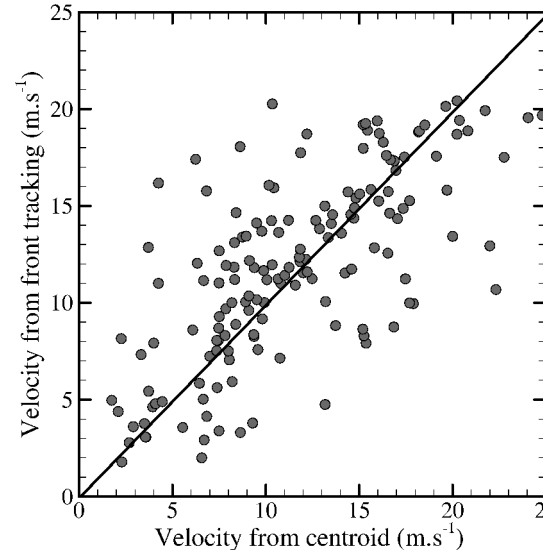


**Fig. 19 Difference between centroid and front tracking velocity.**

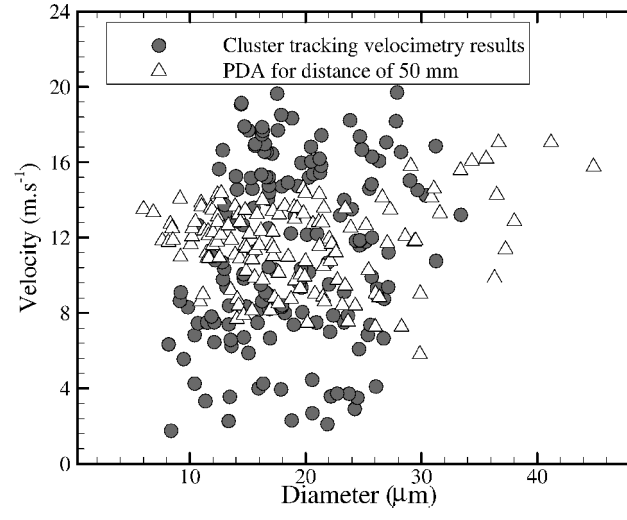


**Fig. 20 Velocities of clusters compared to mean PDA results.**

cluster velocity. This is illustrated in Fig. 17, where the displacement with and without matching of volume is plotted. One can see a small difference in all cases. This is because the laser sheet intensity is quite uniform for both pulses, and, therefore, the threshold levels are almost identical for both images.

Attention is drawn on the uncertainty of the cluster velocity measured by the tracking technique. The uncertainty in determining the displacement of the cluster highly depends on the accuracy of determination of the centroid of the clusters. This is a function of the number of pixels forming the clusters and precision lower than 5 pixels cannot be claimed. This implies that the uncertainty of the cluster velocity is around 3.5 $m \cdot s^{-1}$.

When defining the velocity of the cluster as the displacement of the front boundary of the cluster, the matching of liquid volume between the two displaced images becomes a crucial issue. Figure 18 indicates a large difference in the cluster velocity, when matching and nonmatching of liquid volume in the clusters is used. The comparison between the front boundary tracking and the centroid tracking shows similar behavior when matching the liquid volume in the clusters. The main drawback of taking the front boundary as indicator of the displacement of the cluster is the high sensitivity to the threshold determining the boundary of the cluster. Comparing the two different approaches shows that a discrepancy exists between the computed displacements, as presented in Fig. 19. In summary, the centroid of the cluster should be tracked, as its relative position is not so sensitive (as shown in Fig. 17) to the threshold used to identify the cluster, which is not the case with the front tracking.

The SMD of droplets in a cluster is obtained from the ratio between the total fluorescent intensity within the cluster and the Mie-scattering intensity for the two successive frames. The accuracy of the SMD measurement is high because the size of the clusters is more than 200 pixels; hence, a large number of droplets are considered in the calculation of the value of the SMD. However, PDA measurements provide the velocity of single droplets. To compare the measured size–velocity correlations with the two techniques, the PDA measurements were processed to obtain instantaneous SMD information and velocity by averaging the droplets within fixed time intervals. The measured characteristics of droplets within time intervals of 1 ms, which corresponds to a physical space of 1.5 cm for droplet velocity of 15 $m \cdot s^{-1}$ (the mean velocity at a position 50 mm away from the nozzle), were averaged to provide a value of SMD and corresponding droplet velocity. Figure 20 presents the comparison between size–velocity correlations from PDA and cluster tracking and shows that the measured values fall within a similar interval. After considering the uncertainty of the velocity measurements of the cluster tracking method and the fact that the PDA measurements are averaged over a smaller number of droplets than for the cluster tracking velocimetry, the agreement between the two measurements

is satisfactory. Therefore, the cluster tracking velocimetry can provide correlations between the SMD and velocity of droplet clusters in sprays.

## Conclusions

A technique for planar measurement of droplet size, velocity, liquid volume, and surface area of droplet clusters in sprays is reported. The identification of fluid flow structures, which might be responsible for the formation of the droplet clusters in sprays, is demonstrated. The technique was applied in water sprays with added Rhodamine dye at appropriately adjusted concentration to ensure volume dependency of the fluorescence intensity. The spray was injected in the airflow of a burner for a domestic boiler. Combined droplet laser-induced fluorescence and Mie-scattering intensity images were recorded, using two CCD cameras and appropriate optical filtering, and the ratio of the two light intensity images allowed measurement of instantaneous spatial distribution of droplet Sauter mean diameter (SMD).

It was found that droplet clusters formed in spray regions of high droplet density and low SMD values (lower than 30 $\mu$m) at different instances in time. The identified instantaneous droplet clusters were tracked between time-delayed images, and cross-correlation techniques quantified the instantaneous cluster velocity and measured the droplet cluster SMD-velocity correlation, which agreed well with corresponding phase Doppler droplet size–velocity correlation measurements. In the vicinity of droplet clusters, flow structures were identified, using particle image velocimetry, which might be responsible for the formation of droplet clusters. The fluid flow structures were detected from particle image velocimetry measurements using the Mie-scattering intensity images and were present in regions where low fluorescence intensity was detected, indicating a high concentration of small droplets. The droplet velocity field was measured by cross-correlation techniques from the Mie scattering and fluorescence intensity images and agreed well with the velocity of mean droplet diameters corresponding to the area mean diameter $D_{20}$ and volume mean diameter $D_{30}$ respectively, as measured with the phase Doppler technique. The current findings demonstrate the ability of the planar-droplet-sizing technique to evaluate instantaneous droplet clustering in sprays and identify its origin.

## References

[1]Akamatsu, F., Mizutani, Y., Katsuki, M., Tsushima, S., and Cho, Y. D., "Measurement of the Local Group Combustion Number of Droplet Clusters in a Premixed Spray Stream," *Proceedings of the Twenty-Sixth Symposium on Combustion*, Vol. 26, edited by A. R. Burgess and F. L. Dryer, Combustion Inst., 1996, pp. 1723–1729.

[2]Akamatsu, F., Mizutani, Y., Katsuki, M., Tsushima, S., and Cho, Y. D., "Observation of Combustion Characteristics of Droplet Clusters in a Premixed-Spray Flame by Simultaneous Monitoring of Planar Spray Images and Local Chemiluminescence," *Proceedings of the Twenty-Seventh Symposium on Combustion*, Vol. 27, edited by A. R. Burgess and F. L. Dryer, Combustion Inst., 1998, pp. 1967–1974.

[3]Cao, Z-M., Nishino, K., Mizuno, S., and Torii, K., "PIV Measurement of Internal Structure of Diesel Fuel Spray," *Experiments in Fluids*, Vol. 29, No. 7, 2000, pp. S211–S219.

[4]Engelbert, C., Hardalupas, Y., and Whitelaw, J. H., "Break-Up Phenomena in Coaxial Airblast Atomizers," *Proceedings of the Royal Society of London Series A*, Vol. 451, Jan. 1995, pp. 189–229.

[5]Bachalo, W. D., and Houser, M. J., "Phase/Doppler Spray Analyzer for Simultaneous Measurement of Drop Size and Velocity Distributions," *Optical Engineering*, Vol. 23, No. 5, 1984, pp. 583–590.

[6]Herpfer, D. C., and Jeng, S. M., "Streaked Particle Image Velocimetry and Sizing in a Spray," *Atomization and Sprays*, Vol. 5, Nos. 4–5, 1995, pp. 403–416.

[7]Zimmer, L., "Particle Tracking Velocimetry and Sizing Technique in Two-Phase Flows," *Particle Image Velocimetry and Associated Techniques. Lecture Series 2000–01*, edited by M. L. Riethmuller, von Kàrmàn Inst. for Fluid Dynamics, Brussels, 2000.

[8]Whybrew, A., Nicholls, T. R., Boaler, J. J., and Booth, H. J., "Diode Lasers—a Cost Effective Tool for Simultaneous Visualisation, Sizing and Velocity Measurements of Sprays," *Proceedings of the Fifteenth Annual Conference on Liquid Atomization and Spray Systems*, Inst. for Liquid Atomization and Spray System, Europe, 1999.

[9]Glover, A. R., Skippon, S. M., and Boyle, R. D., "Interferometric Laser Imaging for Droplet Sizing: a Method for Droplet Size Measurements in Sparse Spray Systems," *Applied Optics*, Vol. 34, No. 36, 1995, pp. 8409–8421.

[10]Maeda, M., Kawaguchi, T., and Hishida, K., "Novel Interferometric Measurement of Size and Velocity Distributions of Spherical Particles in Fluid Flows," *Measurement Science and Technology*, Vol. 11, No. 12, 2000, pp. L13–L18.

[11]Yeh, C.-N., Kosaka, H., and Kamimoto, T., "A Fluorescence/Scattering Imaging Technique for Instantaneous 2-D Measurement of Particle Size Distribution in a Transient Spray," *Proceedings of the Third Congress on Optical Particle Sizing*, edited by M. Maeda, Keio Univ., Yokohama, Japan, 1993, pp. 355–361.

[12]Le Gal, P., Farrugia, N., and Greenhalgh, D. A., "Laser Sheet Dropsizing of Dense Sprays," *Optics and Laser Technology*, Vol. 31, No. 1, 1999, pp. 75–83.

[13]Domann, R., and Hardalupas, Y., "A Study of Parameters That Influence the Accuracy of the Planar Droplet Sizing (PDS) Technique," *Particle and Particle Systems Characterization*, Vol. 18, No. 1, 2001, pp. 3–11.

[14]Domann, R., and Hardalupas, Y., "Spatial Distribution of Fluorescence Intensity Within Large Droplets and Its Dependence on Dye Concentration," *Applied Optics*, Vol. 40, No. 21, 2001, pp. 3586–3597.

[15]Ikeda, Y., Yamada, N., and Nakajima, T., "Multi-Intensity-Layer Particle-Image Velocimetry for Spray Measurement," *Measurement Science and Technology*, Vol. 11, No. 6, 2000, pp. 617–626.

[16]Stojkovic, B. D., and Sick, V., "Evolution and Impingement of an Automotive Fuel Spray Investigated with Simultaneous Mie/LIF Techniques," *Applied Physics B*, Vol. 73, No. 1, 2001, pp. 75–83.

[17]Ikeda, Y., Kawahara, N., and Nakajima, T., "Flux Measurements of $O_2$, $CO_2$ and NO in an Oil Furnace," *Measurement Science and Technology*, Vol. 6, No. 6, 1995, pp. 826–832.

[18]Delabroy, O., Lacas, F., Labegorre, B., and Samaniego, J-M., "Parametres de Similitude pour la Combustion Diphasique," *Revue Generale de Thermique*, Vol. 37, No. 11, 1998, pp. 934–953.

[19]Marzouk, Y. M., and Hart, D. P., "Asymmetric Autocorrelation Function to Resolve Directional Ambiguity in PIV Images," *Experiments in Fluids*, Vol. 25, No. 5/6, 1998, pp. 401–408.

[20]Jeong, J., and Hussain, F., "On the Identification of Vortices," *Journal of Fluid Mechanics*, Vol. 285, 1995, pp. 69–94.

[21]Zhou, J., Adrian, R. J., Balachandar, S., and Kendall, T. M., "Mechanisms for Generating Coherent Packets of Hairpin Vortices in Channel Flow," *Journal of Fluid Mechanics*, Vol. 387, 1999, pp. 353–396.

[22]Adrian, R. J., Christensen, K. T., and Liu, Z.-C., "Analysis and Interpretation of Instantaneous Turbulent Velocity Fields," *Experiments in Fluids*, Vol. 29, No. 3, 2000, pp. 275–290.

[23]Raffel, M., Willert, C., and Kompenhans, J., *Particle Image Velocimetry: A Practical Guide*, Springer-Verlag, Heidelberg, Germany, 1998, pp. 147–171.

[24]Domann, R., and Hardalupas, Y., "Characterisation of Spray Unsteadiness," *Proceedings of Eighteenth Annual Conference of Liquid Atomisation and Spray Systems*, Inst. for Liquid Atomization and Spray System, Europe, 2002, pp. 287–292.

R. P. Lucht
*Associate Editor*